JOURNAL OF SOLID STATE CHEMISTRY 118, 280–284 (1995)

Synthesis and Structure of a New Copper(II) Pyroarsenate, $BaCuAs_2O_7$

Tina A. Wardojo and Shiou-Jyh Hwu[1,2]

Department of Chemistry, Rice University, P.O. Box 1892, Houston, Texas 77251

Received February 17, 1995; accepted April 18, 1995

Single crystals of a new barium copper(II) pyroarsenate, $BaCuAs_2O_7$, were grown via an eutectic flux of 40% $BaCl_2$ and 60% NaCl by moles. The structure of this pyroarsenate has been determined by single-crystal X-ray diffraction methods. The title compound crystallizes in the monoclinic system with the space group $P2_1/n$ (No. 14); $Z = 4$. The lattice parameters are $a = 5.740$ (5) Å, $b = 8.475$ (3) Å, $c = 13.090$ (3) Å, $\beta = 91.24$ (4)°, and $V = 636.7$ (6) Å^3. The final least-squares full-matrix refinements yielded $R/R_w = 0.030/0.043$ and GOF = 1.81 for 101 variables. The newly synthesized $BaCuAs_2O_7$ phase is isostructural with $ACuP_2O_7$ (A = Ca, Sr). The unit cell adopts an open framework structure that consists of corner-shared CuO_5 square pyramid and As_2O_7 pyroarsenate groups; Ba atoms occupy the gap between two layered-like $[CuAs_2O_7]$ frameworks. It is recognized, for the first time, that the gap between parallel $[CuAs_2O_7]$ slabs is characterized by a long Cu–O apical bond, 2.386 (3) Å; this length is dictated by the size of the barium cation. In this paper, the flux synthesis, structural analysis, and infrared study of $BaCuAs_2O_7$ are presented.

INTRODUCTION

A wealth of oxy compounds of the AMX_2O_7 family (1 ~ 9) are known for a number of transition metal (M) cations. Most of the pyrophosphates adopt the $A^IM^{III}P_2O_7$ type; where A^I = an alkali metal cation, M = Ti (1), V (2), Fe (3), Y (4), and Mo (5). Scattered examples show the $A^{II}M^{II}P_2O_7$ formulation (6). Compared to the large collection of phosphates, only a few $A^{II}M^{IV}Si_2O_7$ pyrosilicates (7) and $A^IM^{III}As_2O_7$ (8) and $A^{II}M^{II}As_2O_7$ (9) pyroarsenates are known. Despite the wide variety of reported structural types, more novel frameworks are being revealed due to the adaptive nature of the M–O–X–O–M frameworks. With respect to distorted CuO_n (n = 4 ~ 6) coordination geometries, the structural chemistry of copper-based oxy compounds is unique. This has been shown by a large collection of early reports and the recent finding of the $Na_2CuP_2O_7$ compound (10). The latter consists of an unusual wave-like $[CuP_2O_7]_\infty$ ribbon structure.

The current study of the $BaCuAs_2O_7$ compound is an extension of our previous investigations of mixed-framework phosphate and silicate series. The title compound was first synthesized in 1930 as an amorphous precipitate from the aqueous reaction of H_3AsO_4, $CuCO_3$, and $Ba(OH)_2 \cdot 8H_2O$ (11). No further investigative effort on this compound has been reported. In the A–Cu–As–O system, the only other known pyroarsenate was $K_2CuAs_2O_7$, characterized by powder diffraction and infrared spectroscopy methods (12). The present structural analysis shows that it is isostructural with the $ACuP_2O_7$ (A = Ca (6d), Sr (6e)) analogs, and reveals new features concerning the layered framework and the nature of the long Cu–O apical bond.

EXPERIMENTAL

Synthesis. Single crystals of $BaCuAs_2O_7$ were synthesized from As_2O_5 (Aesar, 99.99%), CuO (Strem, 99.999%), and Cu_2O (Aldrich, 97%) in a reaction mixture with the nominal composition Cu_2AsO_4. The total weight of the reactants (charge) was ca. 0.24 g. An eutectic flux (m.p. = 655°C) of 40% $BaCl_2$ (dried from $BaCl_2 \cdot 2H_2O$, EM Science, 99%) and 60% NaCl (EM Science, 99.9%) by moles was ground together in an inert atmosphere dry box. The flux to charge ratio was approximately 5 : 1 by weight. The resulting mixture was loaded into a carbon-coated silica ampoule, which was then sealed under vacuum. The reaction was slowly heated to 800°C and maintained at that temperature for 4 days before it was cooled at 3°C per hour to room temperature. Translucent bluish-green, needle-shaped crystals (approximately 30% yield) were isolated by washing the reaction product with deionized water using a suction filtration method. By-products of the reaction were water soluble.

Structure determination. Diffraction data from an optically pure single crystal were collected at room temperature on a Rigaku AFC5S four-circle diffractometer. Crystallographic data are summarized in Table 1. The unit cell

[1] To whom correspondence should be addressed.

[2] Permanent address: Department of Chemistry, Clemson University, Clemson, SC 29634.

0022-4596/95 $12.00

TABLE 1
Crystallographic Data for $BaCuAs_2O_7$

Formula mass (amu)	462.71
Space group	$P2_1/n$ (No. 14, setting 2)
Cell parameters	
a (Å)	5.740 (5)
b (Å)	8.475 (3)
c (Å)	13.090 (3)
β (degrees)	91.24 (4)
V (Å^3)	636.7 (6)
Z	4
T (K) of data collection	296
ρ calc. (g cm^{-3})	3.56
Radiation (graphite monochromated)	Mo$K\alpha$ (λ = 0.71069 Å)
Crystal shape, color	Needle, bluish-green
Crystal size (mm)	0.01 × 0.02 × 1.0
Linear abs. coeff. (cm^{-1})	169.30
Transmission factors	0.45–1.00
Scan type	ω
Scan speed (deg. min^{-1})	4.0
Scan range (deg.)	−0.36 to 0.36 in ω
Background counts	¼ of scan range on each side of reflection
2θ (max)	55°
Data collected	$h, k, \pm l$
p for σ (F^2)	0.03
No. of reflections measured	1718
No. of unique reflections	1570
No. of unique reflections with $I > 3\sigma(I)$	1278
F_{000}	624
$R(F)^a/R_w(F)^b$/GOF	0.030/0.043/1.81
R_{int}(on $F_0^2 > 3\sigma(F_0^2)$)	0.024
Secondary extinction coefficient	1.22×10^{-6}
No. of variables	101

[a] $R = \Sigma[|F_o| - |F_c|]/\Sigma|F_o|$.
[b] $R_w = [\Sigma w[|F_o| - |F_c|]^2/\Sigma w|F_o|^2]^{1/2}$.

parameters and orientation matrix for data collection were determined by a least-squares fit of 25 peak maxima with $10° < 2\theta < 21°$. According to the intensities of three standard reflections (1, 0, 3; 1, 2, 0; 0, 3, 1), which were measured every 150 reflections, there was no detectable decay during data collection. The TEXSAN software package (13) was used for the crystal structure solution and refinement. Data reduction, intensity analysis, and extinction conditions were determined with the program PROCESS. Lorentz-polarization and empirical absorption corrections based on three computer-chosen azimuthal scans (2θ = 14.22°, 15.02°, 22.96°) were applied to the intensity data. The space group $P2_1/n$ (No. 14, setting 2) was selected on the basis of the extinction conditions. The atomic coordinates of Ba, Cu, and As were determined using the SHELXS-86 program (14), and those of oxygen atoms were resolved by using a difference Fourier map. The structural and thermal parameters were then refined by full-matrix least-squares methods to R = 0.030, R_w = 0.043, and GOF = 1.81. Secondary extinction correction was applied to eliminate poorly matched intense reflections, e.g., $\Delta f/\sigma f > 10$. Table 2 lists the final positional and thermal parameters.

Infrared Spectroscopy. The infrared absorption spectrum of $BaCuAs_2O_7$ was studied in the range 1600 ~ 400 cm^{-1}. The experimental procedures were the same as reported before (10). The peak frequencies corresponding to symmetric (ν_s) and asymmetric (ν_{as}) As–O–As vibrational modes of the $[As_2O_7]$ group are centered at 564 and 786 cm^{-1}, respectively. In addition, the As–O stretching frequencies associated with the $[AsO_4]$ group can be observed at 819 and 892 cm^{-1}. These values are consistent with the characteristic bands for $Na_4As_2O_7$ (15) and $K_2CuAs_2O_7$ (12).

STRUCTURE DESCRIPTION AND DISCUSSION

The $BaCuAs_2O_7$ structure adopts an open framework, as shown in Fig. 1, outlined by Cu–O (thick lines) and As–O (thin lines) bonds. The barium atoms reside in tunnels. Table 3 lists the bond distances and angles illustrating the coordination geometries of three cation-centered polyhedra, i.e., CuO_5, As_2O_7, and BaO_9. The CuO_5 square pyramid shares each of its five corner oxygen atoms with a different As_2O_7 group. The extended lattice is composed of the $[Cu_2(As_2O_7)O_4]$ structural unit, as shown in Fig. 2, the naked oxygen atoms of which are shared with the neighboring units to build up the three-dimensional framework. In Fig. 1, two structural units in each unit cell are related by an inversion center at (½, ½, ½). The O(6) atom of the As_2O_7 pyroarsenate is situated approximately above (or below) the CuO_4 square plane, contributing to the long apical Cu–O bond (omitted for clarity) of the CuO_5 square pyramid.

The elongation of the apical Cu–O bond, although con-

TABLE 2
Positional and Thermal Parameters[a] for $BaCuAs_2O_7$

Atom	x	y	z	B_{eq} (Å^2)
Ba	0.28364(8)	0.15174(6)	0.78624(4)	0.80(2)
Cu	0.2901(2)	0.1411(1)	0.11957(7)	0.81(4)
As (1)	0.8287(1)	0.1832(1)	0.99213(6)	0.63(3)
As (2)	0.2469(1)	0.0338(1)	0.34480(6)	0.63(3)
O (1)	0.661(1)	0.1532(7)	0.6484(5)	1.1(2)
O (2)	0.698(1)	0.0910(8)	0.8923(4)	1.2(2)
O (3)	0.119(1)	0.1488(7)	0.9869(4)	0.9(2)
O (4)	0.296(1)	0.1148(7)	0.4646(4)	1.0(2)
O (5)	0.428(1)	0.1214(7)	0.2632(4)	1.0(2)
O (6)	0.702(1)	0.1601(7)	0.1023(4)	1.1(2)
O (7)	0.971(1)	0.0607(7)	0.3124(5)	1.3(2)

[a] Equivalent isotropic thermal parameters defined as $B_{eq} = (8\pi^2/3)$ trace U.

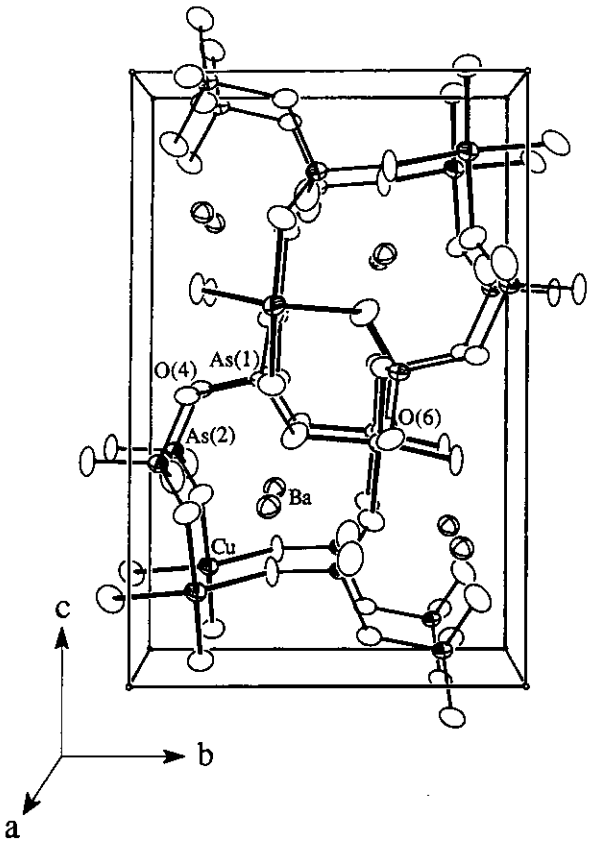

FIG. 1. ORTEP (16) drawing of the perspective view of the $BaCuAs_2O_7$ structure in two unit cells thick. A monoclinic lattice is outlined by solid lines. The $[CuAs_2O_7]$ open framework is highlighted by Cu–O (thick lines) and As–O (thin lines) bonds. Ba atoms (cross-hatched circles) reside in tunnels. Only selected oxygen atoms, O(4) and O(6), are labeled for simplicity. The anisotropic atoms are presented at 90% probability.

sistent with the Jahn–Teller effect due to the Cu(II)-d^9 electron configuration, is dictated by the steric effect of the electropositive cation, Ba^{2+} in this case. Figure 3 shows a partial structure of the layered $[CuAs_2O_7]$ framework with the barium atoms in the gap. This extended framework can be described as layer-like, a feature that is critical to the understanding of the local geometry of the copper cation. The parallel slabs are propagating approximately along the [−101] direction of the unit cell. The separation of two adjacent slabs is characterized by the long apical Cu–O bond distance, e.g., 2.386 (3) Å, presented by dotted lines. Comparisons to the $CaCuP_2O_7$ and $SrCuP_2O_7$ structures suggest that the size of the alkaline-earth cation plays a significant role in determining the apical Cu–O distance, e.g., 2.201 (2) Å and 2.284 (4) Å, respectively. Otherwise, the copper atom is positioned close to the square basal plane with four relatively short Cu–O distances. In the cobalt-containing compounds, $SrCoP_2O_7$ (6b) and $SrCoAs_2O_7$ (9), however, the metal atom (Co) is located near the center of the CoO_5 square pyramid, leading to virtually uniform Co–O distances.

The observed bond distances and angles for CuO_5 and As_2O_7 polyhedra (Table 3) are comparable with reported values. The CuO_5 unit is distorted from an ideal square pyramid as shown by its largely deviated bond angles, e.g., 74.2° and 172.6°. The Cu–O bond distances of the

TABLE 3
Important Bond Distances (Å) and Angles (deg.) for $BaCuAs_2O_7$

	$[CuO_5]$ square pyramid		
Cu^a–$O(1)^b$	1.935(6)	Cu^a–$O(5)^a$	2.030(6)
Cu^a–$O(2)^c$	1.975(7)	Cu^a–$O(6)^a$	2.386(7)
Cu^a–$O(3)^d$	1.978(6)		
$O(1)^b$–Cu^a–$O(2)^c$	158.0(3)	$O(2)^c$–Cu^a–$O(5)^a$	88.7(2)
$O(1)^b$–Cu^a–$O(3)^d$	87.5(3)	$O(2)^c$–Cu^a–$O(6)^a$	91.4(2)
$O(1)^b$–Cu^a–$O(5)^a$	92.1(2)	$O(3)^d$–Cu^a–$O(5)^a$	172.6(2)
$O(1)^b$–Cu^a–$O(6)^a$	110.0(2)	$O(3)^d$–Cu^a–$O(6)^a$	112.9(2)
$O(2)^c$–Cu^a–$O(3)^d$	88.9(2)	$O(5)^a$–Cu^a–$O(6)^a$	74.2(2)
	$[AsO_4]$ tetrahedra		
$As(1)^a$–$O(2)^a$	1.685(6)	$As(2)^a$–$O(1)^c$	1.672(6)
$As(1)^a$–$O(3)^e$	1.694(6)	$As(2)^a$–$O(4)^a$	1.729(6)
$As(1)^a$–$O(4)^f$	1.759(6)	$As(2)^a$–$O(5)^a$	1.678(6)
$As(1)^a$–$O(6)^g$	1.641(6)	$As(2)^a$–$O(7)^h$	1.645(6)
$O(2)^a$–$As(1)^a$–$O(3)^e$	108.1(3)	$O(1)^c$–$As(2)^a$–$O(4)^a$	106.5(3)
$O(2)^a$–$As(1)^a$–$O(4)^f$	104.4(3)	$O(1)^c$–$As(2)^a$–$O(5)^a$	104.7(3)
$O(2)^a$–$As(a)^a$–$O(6)^g$	115.4(3)	$O(1)^c$–$As(2)^a$–$O(7)^h$	116.5(3)
$O(3)^e$–$As(1)^a$–$O(4)^f$	105.1(3)	$O(4)^a$–$As(2)^a$–$O(5)^a$	108.1(3)
$O(3)^e$–$As(1)^a$–$O(6)^g$	118.0(3)	$O(4)^a$–$As(2)^a$–$O(7)^h$	108.3(3)
$O(4)^f$–$As(1)^a$–$O(6)^g$	104.4(3)	$O(5)^a$–$As(2)^a$–$O(7)^h$	112.3(3)
	$As(1)^b$–$O(4)^a$–$As(2)^a$ 125.9(3)		
	$[BaO_9]$ polyhedron		
Ba^a–$O(1)^a$	2.849(6)	Ba^a–$O(6)^i$	2.917(6)
Ba^a–$O(2)^a$	2.777(6)	Ba^a–$O(6)^e$	3.019(6)
Ba^a–$O(3)^a$	2.811(6)	Ba^a–$O(7)^i$	2.684(6)
Ba^a–$O(5)^i$	2.817(6)	Ba^a–$O(7)^e$	2.640(6)
Ba^a–$O(5)^e$	2.928(6)		
$O(1)^a$–Ba^a–$O(2)^a$	70.3(2)	$O(3)^a$–Ba^a–$O(6)^e$	63.1(2)
$O(1)^a$–Ba^a–$O(3)^a$	150.2(2)	$O(3)^a$–Ba^a–$O(7)^i$	91.8(2)
$O(1)^a$–Ba^a–$O(5)^i$	119.3(2)	$O(3)^a$–Ba^a–$O(7)^e$	104.9(2)
$O(1)^a$–Ba^a–$O(5)^e$	54.7(2)	$O(5)^i$–Ba^a–$O(5)^e$	158.24(8)
$O(1)^a$–Ba^a–$O(6)^i$	65.5(2)	$O(5)^i$–Ba^a–$O(6)^i$	55.6(2)
$O(1)^a$–Ba^a–$O(6)^e$	107.3(2)	$O(5)^i$–Ba^a–$O(6)^e$	131.4(2)
$O(1)^a$–Ba^a–$O(7)^i$	76.6(2)	$O(5)^e$–Ba^a–$O(6)^i$	109.3(2)
$O(1)^a$–Ba^a–$O(7)^e$	96.6(2)	$O(5)^e$–Ba^a–$O(6)^e$	53.5(2)
$O(2)^a$–Ba^a–$O(3)^a$	80.4(2)	$O(5)^i$–Ba^a–$O(7)^i$	71.5(2)
$O(2)^a$–Ba^a–$O(5)^i$	142.3(2)	$O(5)^i$–Ba^a–$O(7)^e$	91.1(2)
$O(2)^a$–Ba^a–$O(5)^e$	58.7(2)	$O(5)^e$–Ba^a–$O(7)^i$	121.2(2)
$O(2)^a$–Ba^a–$O(6)^i$	129.4(2)	$O(5)^e$–Ba^a–$O(7)^e$	70.3(2)
$O(2)^a$–Ba^a–$O(6)^e$	65.3(2)	$O(6)^i$–Ba^a–$O(6)^e$	151.6(2)
$O(2)^a$–Ba^a–$O(7)^i$	76.5(2)	$O(6)^i$–Ba^a–$O(7)^i$	70.5(2)
$O(2)^a$–Ba^a–$O(7)^e$	125.3(2)	$O(6)^i$–Ba^a–$O(7)^e$	83.8(2)
$O(3)^a$–Ba^a–$O(5)^i$	81.3(2)	$O(6)^e$–Ba^a–$O(7)^i$	136.6(2)
$O(3)^a$–Ba^a–$O(5)^e$	113.8(2)	$O(6)^e$–Ba^a–$O(7)^e$	69.4(2)
$O(3)^a$–Ba^a–$O(6)^i$	136.5(2)	$O(7)^i$–Ba^a–$O(7)^e$	154.0(2)

Note. Symmetry codes: ^{a} $+x, +y, +z$; ^{b} $-\frac{1}{2}+x, \frac{1}{2}-y, -\frac{1}{2}+z$; ^{c} $1-x, -y, 1-z$; ^{d} $x, y, -1+z$; ^{e} $1+x, +y, +z$; ^{f} $\frac{1}{2}+x, \frac{1}{2}-y, \frac{1}{2}+z$; ^{g} $+x, +y, 1+z$; ^{h} $-1+x, +y, +z$.

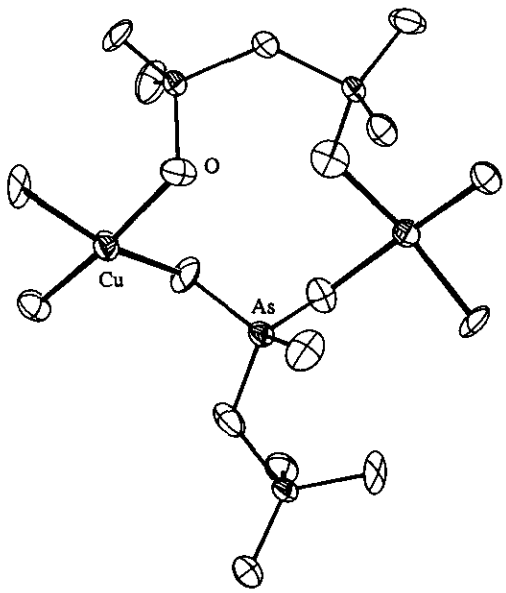

FIG. 2. ORTEP drawing of the $[Cu_2(As_2O_7)_2O_4]$ structural unit. The apical oxygen with respect to each copper atom is omitted for clarity. The anisotropic atoms are presented at 90% probability.

basal plane are in the range 1.94 ~ 2.03 Å, comparable to the ranges 1.92 ~ 2.04 Å and 1.91 ~ 2.05 Å of the Ca and Sr pyrophosphate analogs, respectively. The AsO_4 tetrahedral coordination is slightly distorted on the basis of its nearly regular bond angles, e.g., 104.4° ~ 118.0°. The As(1)–O(4)–As(2) angle for the As_2O_7 pyroarsenate is as close as 125.9° due to a staggered configuration (Fig. 3). The As–O bridging/terminal bond distances are 1.73 ~ 1.76 Å/1.64 ~ 1.69 Å, which are comparable to the distances 1.79 ~ 1.80 Å/1.65 ~ 1.67 Å of the $CaK_2As_2O_7$ structure, taking into account a small As–O–As angle, e.g., 120.9° (17).

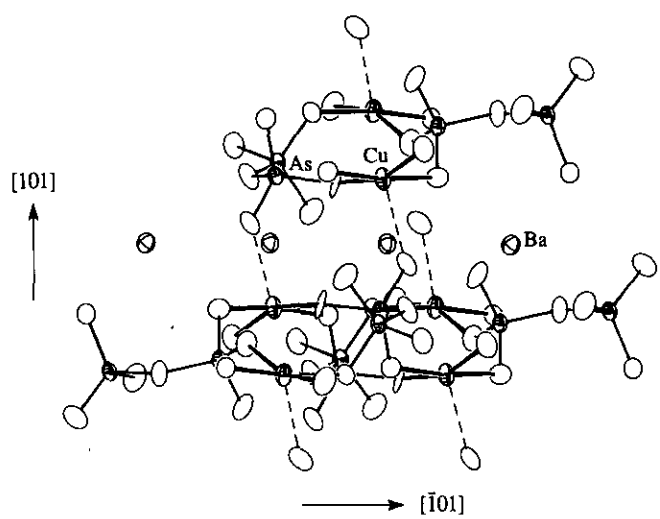

FIG. 3. Partial structure of the layered $[CuAs_2O_7]$ framework with barium atoms in the gap. For clarity, there is only one structural unit drawn for the top slab and two are drawn for the bottom one. The oxygen atoms are in open circles. The dotted lines represent long apical Cu–O bonds. The anisotropic atoms are presented at 90% probability.

There is no direct Cu–Cu interaction, as might be expected because of the layered framework. The d_{Cu-Cu} is far beyond the Cu–Cu distance in the f.c.c. metallic copper, e.g., 2.57 Å (18). The longest d_{Cu-Cu} is 5.74 Å along a ($d_{Cu-Cu} \equiv a$), while the shortest d_{Cu-Cu} is 4.65 Å across the origin of the unit cell. Two intermediate ones are 5.12 Å across the inversion center at $(\frac{1}{2}, \frac{1}{2}, \frac{1}{2})$ and 5.47 Å between copper atoms from approximately one side of Ba to the other.

As in any other oxy compounds, the incorporated electropositive cation governs the structural formation by means of keeping charges balanced. The barium cation adopts an irregular BaO_9 coordination, in which the average Ba–O distance is 2.83 Å, similar to 2.89 Å, the sum of Shannon crystal radii (19) of 9-coordinated Ba^{2+} (1.61 Å) and O^{2-} (1.28 Å). Based upon the bond valence sum (BVS) analysis (20), the formal oxidation states have been calculated to be 2.18, 1.93, and 4.89/5.06 for Ba, Cu, and As atoms, respectively. On the basis of the O^{2-} formal oxidation state, the charge distribution for the title compound can be formulated as $Ba^{II}Cu^{II}As_2O_7$, an additional member of the $A^{II}M^{II}X_2O_7$ type.

In summary, the construction of each structural unit is fascinating due to the adaptive bond interactions of polyhedra, CuO_5 and As_2O_7 in this case, and the size/charge of the electropositive cation incorporated. Curiously enough, $BaCuAs_2O_7$ is isostructural with neither $BaCoP_2O_7$ (6c) nor $BaCuP_2O_7$ (6f), both of which crystallized in a triclinic unit cell, and in which the Cu^{2+} atoms bridge two successive P_2O_7 groups. Synthetically, the eutectic flux method facilitates different conditions for crystal growth than hydrothermal and conventional solid-state approaches. Therefore, more interesting frameworks are anticipated.

ACKNOWLEDGMENT

Financial support for this research (DMR-9208529) and the single-crystal X-ray diffractometer from the National Science Foundation are gratefully acknowledged.

REFERENCES

1. (a) $LiTiP_2O_7$: S. Wang and S.-J. Hwu, Rice University, Houston, Texas, unpublished research (1990). (b) α-, β-$NaTiP_2O_7$: A. Leclaire, A. Benmoussa, M. M. Borel, A. Grandin, and B. Raveau, *J. Solid State Chem.* **77,** 299 (1988), (c) (K, Rb, Cs)TiP_2O_7: S. Wang and S.-J. Hwu, *J. Solid State Chem.* **92,** 219 (1991).
2. (a) $LiVP_2O_7$: K. H. Lii, Y. P. Wang, and Y. B. Chen, *J. Solid State Chem.* **86,** 143 (1990), (b) $NaVP_2O_7$: Y. P. Wang, K. H. Lii, and S. L. Wang, *Acta Crystallogr. Sect. C* **45,** 673 (1989), (c) $CsVP_2O_7$: Y. P. Wang and K. H. Lii, *Acta Crystallogr. Sect. C* **45,** 1210 (1989).

3. (a) $LiFeP_2O_7$: E. A. Genkina, B. A. Maksimov, V. A. Timofeeva, A. B. Bykov, and O. K. Mel'nikov, *Sov. Phys. Dokl.* **30**(10), 817 (1985), (b) $NaFeP_2O_7$: M. Gabelica-Robert, M. Goreaud, Ph. Labbe, and B. Raveau, *J. Solid State Chem.* **45,** 389 (1982), (c) $KFeP_2O_7$: D. Riou, Ph. Labbe, and M. Goreaud, *Eur. J. Solid State Inorg. Chem.* **25,** 215 (1988), (d) $AFeP_2O_7$ (A = Rb, Cs): E. Dvoncova and K.-H. Lii, *J. Solid State Chem.* **105,** 279 (1993).
4. KYP_2O_7: A. Hamady, M. F. Zid, and T. Jouini, *J. Solid State Chem.* **113,** 120 (1994).
5. (a) $NaMoP_2O_7$: A. Leclaire, M. M. Borel, A. Grandin, and B. Raveau, *J. Solid State Chem.* **76,** 131 (1988), (b) $KMoP_2O_7$: A Leclaire, M. M. Borel, A. Grandin, and B. Raveau, *J. Solid State Chem.* **78,** 220 (1989), (c) $RbMoP_2O_7$: unpublished work cited in K.-H. Lii, C. C. Wang, and J. J. Chen., *J. Solid State Chem.* **78,** 93 (1989), (d) $CsMoP_2O_7$: K.-H. Lii and R. C. Haushalter, *Acta Crystallogr. Sect. C* **43,** 2036 (1987).
6. (a) $CaCoP_2O_7$: D. Riou, P. Labbe, and M. Goreaud, *C.R. Acad. Sci. Paris* **307,** 1751 (1988), (b) $SrCoP_2O_7$: D. Riou and B. Raveau, *Acta Crystallogr. Sect. C* **47,** 1708 (1991), (c) $BaMP_2O_7$ (M = Co, Ni): D. Riou, P. Labbe, and M. Goreaud, *C.R. Acad. Sci. Paris* **307,** 903 (1988), (d) $CaCuP_2O_7$: D. Riou and M. Goreaud, *Acta Crystallogr. Sect. C* **46,** 1191 (1990), (e) $SrCuP_2O_7$: A. Moqine, A. Boukhari, L. Elammari, and J. Durand, *J. Solid State Chem.* **107,** 368 (1993), (f) $BaCuP_2O_7$: A. Moqine and A. Boukhari, *Acta Crystallogr. Sect. C* **47,** 2294 (1991).
7. (a) β-$BaTiSi_2O_7$: N. Köpper and Dietzel, *Glastech. Ber.* **49,** 199 (1976), (b) α-$BaVSi_2O_7$: S. Matsubara, A. Kato, and S. Yui, *Mineral. J.* **11,** 15 (1982), (c) $BaVSi_2O_7$: A. Feltz, S. Schmalfuss, H. Langbein, and M. Tietz, *Z. Anorg. Allg. Chem.* **417,** 125 (1975), (d) β-$BaVSi_2O_7$: G. Liu and J. E. Greedan, *J. Solid State Chem.* **108,** 267 (1994), (e) $SrVSi_2O_7$: Y. Takeuchi and W. Joswig, *Mineral. J.* **5,** 98 (1967).
8. $LiFeAs_2O_7$: S.-L. Wang, C.-H. Wu, and S.-N. Liu, *J. Solid State Chem.* **113,** 37 (1994).
9. $SrCoAs_2O_7$: J.-C. Horng and S.-L. Wang, *Acta Crystallogr. Sect. C* **50,** 488 (1994).
10. K. M. S. Etheredge and S.-J. Hwu, *Inorg. Chem.* **34,** 1495 (1995). [And references therein]
11. A. Rosenheim and H. Antelmann, *Z. Anorg. Allg. Chem.* **193,** 73 (1930).
12. M. Gabelica-Robert, *C.R. Acad. Sci. Paris* **293,** 497 (1981).
13. (a) "TEXSAN: Single Crystal Analysis Software, Version 5.0," Molecular Structure Corp., The Woodlands, TX (1989); (b) Scattering factors for nonhydrogen atoms: D. T. Cromer, and J. T. Waber, *in* "International Table for X-Ray Crystallography," Vol. IV, Table 2.2A, pp. 71–98, Kynoch Press, Birmingham, UK (1974).
14. G. M. Sheldrick, *in* "Crystallographic Computing 3" (G. M. Sheldrick, C. Krüger, and R. Goddard, Eds.), pp. 175–189. Oxford University Press, London/New York (1985).
15. K. Nakamoto, *in* "Infrared and Raman Spectra of Inorganic and Coordination Compounds," 4th ed. Wiley, New York, 1986.
16. C. K. Johnson, "*ORTEP II*," Report ORNL-5138, Oak Ridge National Laboratory, Oak Ridge, TN (1976).
17. R. Faggiani and C. Calvo, *Can. J. Chem.* **54,** 3319 (1976).
18. D. R. Lide, *in* "Handbook of Chemistry and Physics," 71st ed. CRC Press, Boston, 1990.
19. R. D. Shannon, *Acta Crystallogr. A* **32,** 751 (1976).
20. (a) I. D. Brown and D. Altermatt, *Acta Crystallogr. B* **41,** 244 (1985). (b) N. E. Brese and M. O'Keefe, *Acta Crystallogr. B* **47,** 192 (1991).